Thin Solid Films 636 (2017) 107–115

Contents lists available at ScienceDirect

Thin Solid Films

journal homepage: www.elsevier.com/locate/tsf

Copper-graphene oxide composite coatings for corrosion protection of mild steel in 3.5% NaCl

Y. Raghupathy, Anshul Kamboj, RekhaM.Y., Narasimha RaoN.P., Chandan Srivastava *

Department of Materials Engineering, Indian Institute of Science, Bangalore, India

ARTICLE INFO

Article history:
Received 30 November 2016
Received in revised form 26 April 2017
Accepted 26 May 2017
Available online 27 May 2017

Keywords:
Graphene oxide
Coatings
Electrodeposited
Corrosion
Texture

ABSTRACT

This paper investigates the effect of graphene oxide (GO) on morphology, microstructure and corrosion behaviour of Cu-GO composite coatings. Cu-GO composite coatings were electrodeposited on mild steel substrate by dispersing chemically synthesised GO into a Cu electrolytic bath. Anionic surfactant (sodium lauryl sulphate) was used to obtain uniform and compact coating morphology. Incorporation of GO into Cu matrix produced a finer granular coating morphology with a strong ⟨220⟩ preferred orientation. The analysis of electrochemcial corrosion test results revealed that steels coated with Cu-GO were invariably more corrosion resistant compared to both bare steel and pure Cu coated steel. Extent of the reduction in the corrosion rate increased with increasing amount of GO in electrodeposited Cu matrix. Improved corrosion resistance of Cu-GO coatings was related to ⟨220⟩ texture and high impermeability of GO to Cu^{+} ions and dissolved O_2 in the chloride media.

1. Introduction

Graphene and graphene oxide (GO) have attracted considerable attention owing to their unique physicochemical properties and ease of synthesis [1–4]. Corrosion inhibition of metals using graphene [5–8] and graphene based composite coatings [9–19] is an emerging area of major practical interest. For instance, ultrathin graphene layers grown on steel [5,6], Cu [7], Ni [7,8] and metal-graphene composite coatings such as graphene-Cr [18] and graphene-Sn [19] have been shown to protect the underlying metals very effectively against corrosive attack. Between pristine graphene coating and metal-graphene composite coatings, the former is highly prone to defects upon prolonged use leading to localised attack of the underlaying substrates [7,20,21]. On the other hand, graphene or graphene oxide incorporated into a suitable metal matrix can produce relatively stable composite coatings for long-term engineering applications. However, limited dispersibility exhibited by graphene in water can severely limit formation of uniform metal-graphene composite coatings on a large area substrate [22]. Hydrophilic graphene oxide which is basically graphene sheet decorated with several oxygenated functional groups (hydroxyl, epoxy, carbonyl etc.) exhibit excellent dispersibility in water making them more suited for uniform large scale coatings [22].

In this paper, nanocrystalline Cu-GO composite coatings electrodeposited on mild steel were studied with regard to their electrochemical corrosion behaviour in 3.5% NaCl. Corrosion of steels is a major threat to their engineering applications [23,24]. There is therefore a need to explore new alternatives to conventional zinc based coatings [25,26]. Cu is well-known for its sea water applications due to its corrosion resistance [27–29] and anti-fouling properties [30]. However, use of Cu coatings on steel is mostly restricted to electronic and decorative applications [31,32]. Electrodeposition presents a relatively simple and scalable coating technology for Cu [33]. In this study, the morphology, texture and corrosion behaviour of electrodeposited Cu coatings were investigated as a function of GO content.

2. Experimental

2.1. Synthesis of graphene oxide

GO was prepared using modified Hummer's method [34]. A reaction mixture was prepared by adding 75 ml of concentrated H_2SO_4 to a mixture of graphite powder (200 mesh, 99.99% metal base, 2 g) and $NaNO_3$ (2 g). Controlled oxidation of the graphite resulted when $KMnO_4$ (6 g) was added slowly into the above reaction mixture cooled to a temperature below 5 °C under constant agitation. After 24 h long stirring, the reaction mixture was heated to and held at 35 °C and 98 °C for 15 min each before cooling to the room temperature. Compared to the conventional Hummer's method, the modified approach essentially employed long stirring times (up to 24 h) in order to promote the oxidation of graphite. Oxidation of graphite was discontinued by addition of de-ionised (DI) water and 30% (w/v) H_2O_2. The reaction mixture was diluted several times with DI water in order to obtain a stable dispersion of GO in DI water.

* Corresponding author.
E-mail address: csrivastava@materials.iisc.ernet.in (C. Srivastava).

http://dx.doi.org/10.1016/j.tsf.2017.05.042
0040-6090/

2.2. Electrodeposition

A DC current source was used to electrochemically grow pure Cu and Cu-graphene oxide (Cu-GO) coatings on mild steel (MS) substrates (%C: 0.23, %Mn: 1.2, %S < 0.1, %P < 0.1 & %Fe ≈ 98.4). Initially, MS coupons were polished with SiC abrasives, pickled in 10% (v/v) HCl solution and washed using a jet of tap water in order to achieve a clean and metallic surface. Depositions were conducted in a rectangular cell with MS (20 mm × 20 mm × 0.5 mm) as cathode and platinum foil (25 mm × 25 mm × 0.53 mm) as anode. Basic electroplating bath consisted of hydrated copper sulphate as a source of Cu^{2+} ions and sodium lauryl sulphate (SLS) as a surfactant. Different Cu-GO composite coatings were electrodeposited by dispersing different amounts of GO in the basic electroplating bath. All the coatings including pure Cu were electrodeposited using the same SLS concentration in order that corrosion behaviour of the coatings can be studied as a function of GO content alone. The optimized bath chemistry and the plating conditions used for electrodeposited coatings are summarized in the Table 1.

2.3. Electrochemical corrosion testing and characterisation

As-prepared GO was characterised using Raman spectroscopy (LabRaman HR system, 532 nm LASER), UV–Vis spectroscopy (Perkin Elmer Spectrometer, Lambda 35), and X-ray diffraction (PANalytical JDX-8030 diffractometer, Cu K_α X-ray source and X-ray photoelectron spectroscopy (Kratos Axis Ultra, monochromatic Al K_α source). Scanning electron microscopy (ESEM QUANTA 200, FEI) was used to obtain the morphology of as-prepared GO and electrodeposited coatings. A CHI electrochemical workstation (CHI Instruments, 604E) was employed to investigate electrochemical corrosion behaviour of the coatings. Electrochemical measurements were performed in a conventional three-electrode cell with aerated 3.5% NaCl (pH 7) as the electrolyte. The electrochemical cell set-up consisted of 1 cm^2 area of the as-deposited coating as the working electrode, platinum foil (30 mm × 25 mm × 0.4 mm) as the auxiliary electrode and Ag-AgCl (saturated KCl) as the reference electrode.

3. Results and discussion

3.1. Analysis of as-synthesised GO

The Hummer's protocol yielded stable dispersions of GO with a characteristic yellow colour indicating successful oxidation of graphite during the synthesis reaction [2,4]. This was confirmed by analysis of the XRD pattern, UV–Vis spectra, Raman Spectra, and XPS spectra obtained from as-prepared GO samples (Fig. 1a–d). In Fig. 1a, a sharp peak centered at 2θ = 11.45° was ascribed to the (001) crystal plane [4,5] with an enlarged d spacing (d spacing) of ≈0.77 nm as compared to the d spacing in the graphite (≈0.33 nm) [35]. Enlarged d spacing in GO was due to intercalation of oxygenated functional groups such as hydroxyl, epoxy, carbonyl etc. between graphitic layers [4]. The inset (Fig. 1a) is a SEM micrograph showing chemically exfoliated GO platelets.

In the UV–Vis spectrum in Fig. 1b, an absorption maximum (**A**) at 235.5 nm and a shoulder peak (**B**) at 300 nm (Fig. 1b) are attributed to π-π* transition of aromatic C—C bonds (of GO) and n-π* transition of C═O bonds (of GO) respectively [2–4]. The sharp absorption peak (**A**) also ascertained that the as-prepared GO was highly dispersible in polar solvents such as water due to polar oxygen functional groups in GO [2]. Raman spectra in Fig. 1c and C1s spectra (Fig. 1d) provided structural information about GO. The Raman spectra showed G band (≈1608 cm^{-1}), D band (≈1354 cm^{-1}) with large and comparable intensities. Both G and D bands refer to first order phonon vibration of sp^2 C, and are a common feature in Raman spectra of GO. While G refers to in-plane stretching of sp^2 C pairs in rings and chains, D band corresponds to a breathing mode vibration of aromatic rings activated by structural defects in graphitic structure [2,4]. Various functional groups attached to the basal planes and edges in graphene produce lattice distortions leading to a pronounced D band [2]. Additionally, a weak and broad 2D band at 2656 cm^{-1} is overtone of D band and is caused by second order two-phonon mode lattice vibration [2]. Chemically exfoliated GO is typically characterised by pronounced D band and a broad 2D band [2]. A weak D + G band at 2915 cm^{-1} is again believed to be due to defects in GO [2]. C1s spectrum (Fig. 1d) of GO was deconvoluted into three component peaks corresponding to characteristic carbon bonds, namely C in aromatic ring (C═C, 284.4 eV), epoxy/alkoxy (C—O, 286.4 eV) and carbony (C═O, 287.8 eV) [4,22]. The peak intensity values of C═C and C—O bonds were found to be 50.7% and 49.3% respectively. This demonstrated successful oxidation of graphite during synthesis.

3.2. Morphology and microstructure of pure Cu and Cu-GO coatings

Addition of GO into the Cu plating bath produced Cu-GO composite coatings on MS substrate. Cu-GO1, Cu-GO2 and Cu-GO3 were the composite coatings deposited from bath B1, B2 and B2 respectively. SLS (sodium lauryl sulphate) bath concentration, cathodic current density and pH were optimized to obtain coatings with highly compact and granular morphology (Fig. 2). From the SEM micrographs of substrate-coating cross section, the average coating thickness of pure Cu and Cu-GO composite coatings was found to be 25 ± 3 μm.

Cu plating from sulphate bath is usually limited to a narrow pH range, i.e. 1–3 [36]. Compactness and uniformity of the electrodeposited coatings can be mainly attributed to presence of SLS in the plating bath. Being an anionic surfactant, SLS is known to, (a) improve the wettability of substrate to be coated [37], and (ii) prevent the agglomeration of nanoparticles in the bath (GO in the present case) by adsorbing preferentially to the nanoparticles [38,39]. From Fig. 2, it can be inferred that GO in electrodeposited Cu led to a mild refinement in the granular morphology compared to the morphology of the pure Cu coatings. Cu and Cu-GO coatings showed no significant difference with respect to XRD peak positions (Fig. 3a). The XRD peaks at 43.4°, 50.5° and 74.2° matched with (111), (200) and (220) crystal planes of fcc Cu. The peaks at 44.7° and 65.1° matched with (110) and (200) crystal planes of bcc ferrite (MS). Crystallite size of Cu was about 45, 41, 41, and 40 nm for Cu, Cu-GO1, Cu-GO2 and Cu-GO3 respectively as determined

Table 1
Optimized plating conditions.

Plating bath	Bath constituents	Concentration (g L^{-1})	Coating	Operating parameters
Primary bath (B)	$CuSO_4 \cdot 5H_2O$	120	Cu	Anode: Platinum foil (25 mm × 25 mm × 0.53 mm)
	SLS (sodium lauryl sulphate)	0.288		Cathode: Mild steel
				Cathodic current density: 25 mA cm^{-2}
				Deposition time: 10 min
B1	B + GO	0.125	Cu-GO1	Cl^- content (using HCl): 35 ppm
B2	B + GO	0.25	Cu-GO2	pH: 2.4
B3	B + GO	1	Cu-GO3	Bath temperature: 25 ± 2 °C

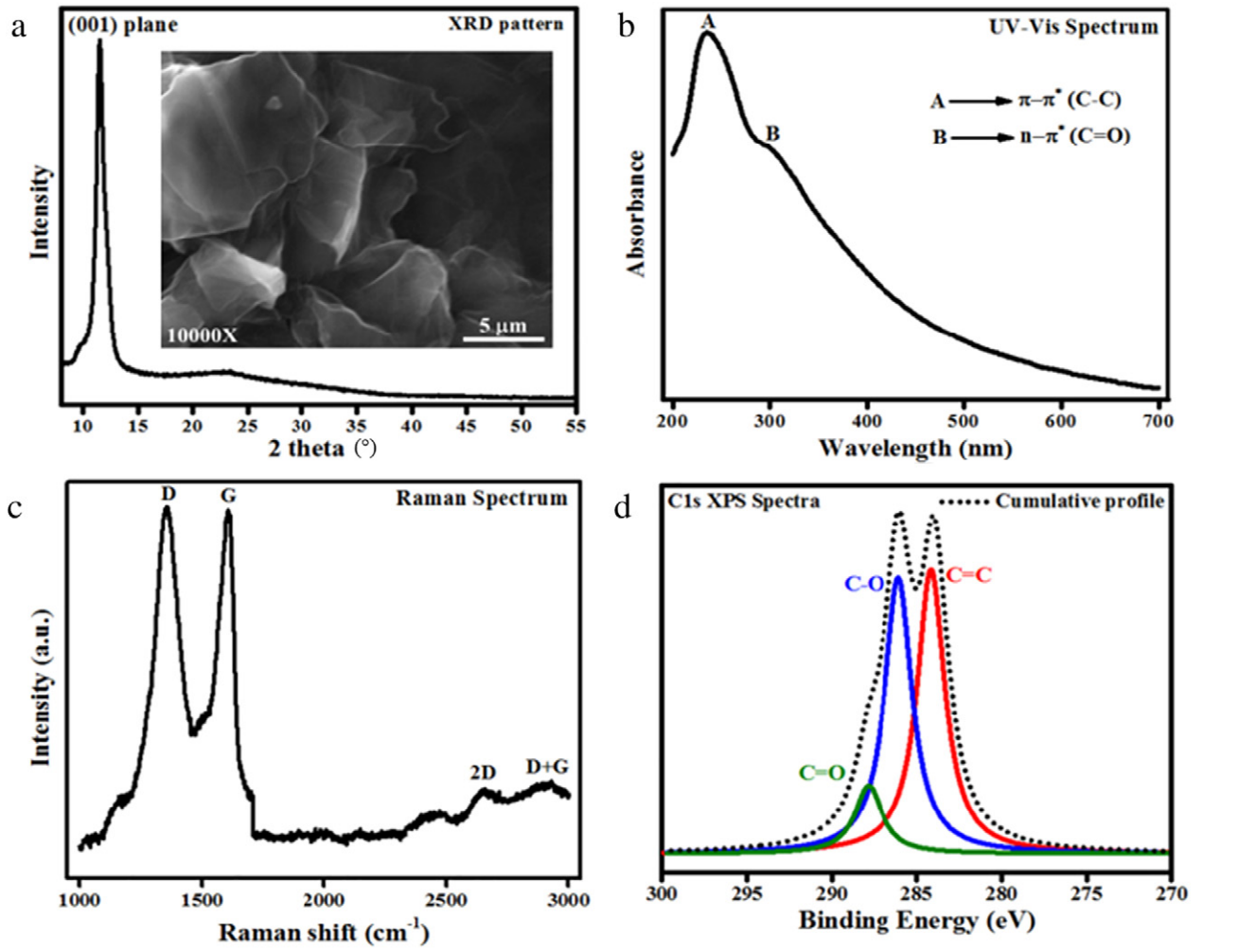

Fig. 1. (a) XRD pattern, (b) UV–Vis spectra, (c) Raman spectra, and (d) C1s XPS spectra recorded from as-prepared GO. Inset in (a) is a representative SEM micrograph of GO platelets.

by the Scherrer analysis [40] of the (111) peak of Cu. Texture co-efficient (T_c) was calculated from XRD peak intensity as described below [23].

$$T_c(hkl) = \frac{I_{hkl}}{\sum I_{hkl}} \times \frac{\sum I_{0hkl}}{I_{0hkl}} \quad (1)$$

where, I_{hkl} and $I_{0(hkl)}$ refer to the (hkl) peak intensity from the coating and a standard reference pattern respectively. From Fig. 3b, it is evident that GO strongly favoured crystal growth along ⟨220⟩ directions and suppressed growth along ⟨111⟩ and ⟨200⟩ directions. It can be due to a modification of cathodic surface energy caused by GO adsorption on to MS cathode during electroplating [23]. Modified surface morphology of Cu-GO coatings may be related to change in the growth tendencies of different atomic planes caused by GO [41].

3.3. Electrochemical corrosion behaviour of coatings

Electrochemical corrosion behaviour of bare steel and coated steels was determined using Tafel polarization studies in 3.5% NaCl medium. Tafel tests were performed by polarizing the working electrode ±200 mV from the respective open circuit potential values. Each measurement was performed thrice in order to verify the reproducibility of results. Tafel polarization curves obtained from bare MS and MS coated with Cu and Cu-GO are shown in Fig. 4. Electrochemical parameters derived from the corrosion tests are given in Table 2. Bare MS, Cu/MS (i.e. Cu coated on MS), Cu-GO1/MS, Cu-GO2/MS and Cu-GO3/MS produced corrosion potential (E_{corr}) values of −0.648 V, −0.579 V, −0.537 V, −0.505 V and −0.321 V respectively. It can be easily seen that, when compared to bare MS, the coated MS samples consistently yielded greater corrosion potential (E_{corr}). Additionally, E_{corr} was found to increase with increasing GO content. The corrosion current density (i_{corr}) values obtained from bare MS, Cu/MS, Cu-GO1/MS, Cu-GO2/MS and Cu-GO3/MS were 295.3, 62.89, 21.28, 11.13 and 7.24 μA cm^{-2} respectively. Reduction in i_{corr} with increasing GO content was consistent with increase in E_{corr}. The results clearly showed that both Cu and GO were effective in inhibiting the extent of corrosion in Cl^- environment. Whenever a decrease in the extent of corrosion is associated with an increase in E_{corr}, the overall corrosion process (which comprises oxidation and reduction reactions) is said to be controlled by rate of anodic oxidation reaction [42–44]. Cu corrosion in aerated Cl^- media can be described as follows [45,46].

$$Cu_{coating} + 2Cl^-_{aq} \leftrightarrow CuCl^-_{2\,(aq)} + \bar{e}\ldots \quad (3.1)$$

$$Cu_{coating} \leftrightarrow Cu^+_{aq} + \bar{e}\ldots \quad (3.2)$$

$$Cu^+_{aq} + 2Cl^-_{aq} \leftrightarrow CuCl^-_{2\,(aq)}\ldots \quad (3.3)$$

The above reaction given in Eq. (3.1) can be divided up into its constituent reactions (3.2) and (3.3). Reaction (3.2) is the main oxidation reaction of Cu in Cl^- media. Cu, when exposed to an aqueous system of Cl^- ions, is known to dissolve as Cu^+ ions due to the formation of thermodynamically stable complex ions, i.e. $CuCl^-_2$ in water.

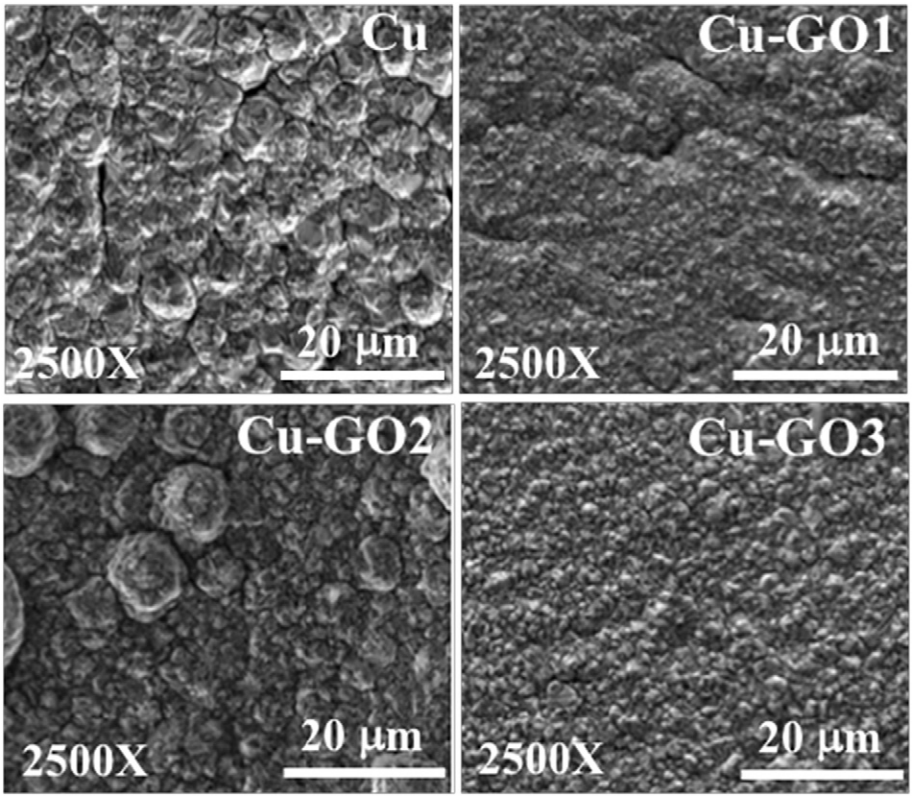

Fig. 2. Surface morphology of electrodeposited Cu and Cu-GO coatings.

For Cu in aerated Cl^- solution at neutral pH, oxygen reduction is the primary cathodic reaction as described below [27].

$$O_2 + 2H_2O + 4\bar{e} \leftrightarrow 4OH^- \ldots \quad (3.4)$$

The corrosion rate (CR) was calculated using the following equation [44].

$$CR(mpy) = \frac{0.129 \times i_{corr} \times M}{z \times \rho} \ldots \quad (2)$$

where M is the atomic weight of metal, z the number of electrons that is lost per metal atom during anodic dissolution of metal, and ρ the density of the metal undergoing corrosion.

CR values of bare MS, Cu/MS, Cu-GO1/MS, Cu-GO2/MS and Cu-GO3/MS were found to be 135.15, 57.53, 19.46, 10.18 and 6.62 mpy respectively. Reduction in the susceptibility of the coated steels to Cl^- attack indicated the protective nature of electrodeposited Cu and Cu-Go coatings. Furthermore, the evaluated corrosion rate numbers showed that the reduction in the corrosion rate of Cu due to addition of GO1, GO2 and GO3 was about 66%, 82% and 88% respectively. These results demonstrated that addition of small amounts of GO in Cu matrix can be

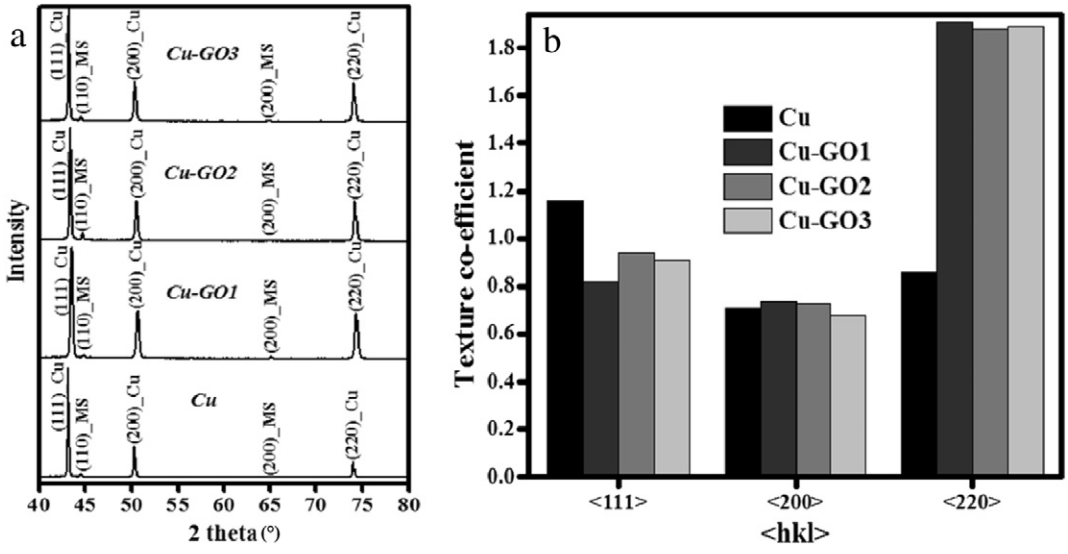

Fig. 3. (a) XRD patterns of the coatings, (b) texture co-efficient of coatings calculated from XRD peak intensities.

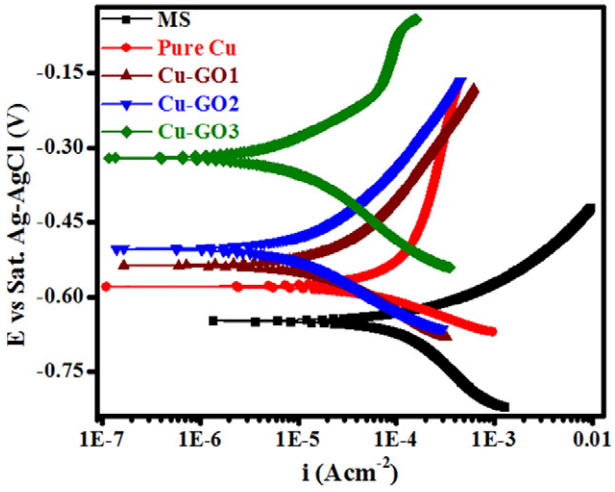

Fig. 4. Tafel polarization curves obtained from bare MS and MS coated with Cu and Cu-GO.

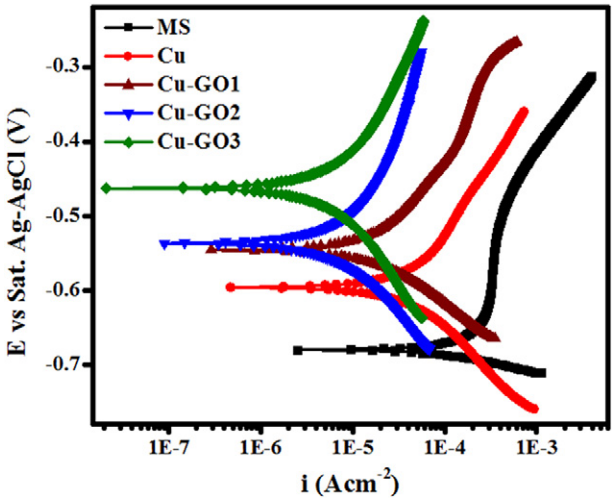

Fig. 5. Tafel polarization curves obtained from bare MS, pure Cu, and Cu-GO coatings after their 5 day exposure to 3.5% NaCl.

used to improve the corrosion resistance of Cu significantly. The obtained results on corrosion can be further discussed based on the surface passive films on nanocrystalline coatings and entrapped GO within coating microstructure. It is already well established that Cu and Cu based materials are invariably characterised by thin surface passive films whose structure, composition, and thickness depend mainly on material's microstructure in a given environment [27,47]. Formation of such passive films on Cu is further promoted by nanocrystalline microstructure [48,49]. These films are generally known to protect the underlying Cu metal from corrosion [27,50,51]. A large body of literature suggests that, for Cu exposed to neutral and aerated Cl^- media, the passive layer is comprised primarily of Cu_2O [27,46–51]. Presence of passive films on Cu and Cu-GO coatings was indicated by the anodic Tafel slopes (Table 2) which were appreciably larger than 60 mV/decade which is average value of anodic slope for freshly polished Cu, namely Cu surface with no passive film [27,52].

Improved corrosion resistance of the Cu-GO composite coatings can be explained based on surface passive layer in the as-deposited state, and high impermeability of GO. It is envisaged that increased surface energy due to ⟨220⟩ texture can lead to enhanced passive film formation on Cu-GO composite coatings. It is worth noting that, for a passive metal such as Cu, extent of passivity and tendency for electrochemical corrosion is generally found to be dependent on crystallographic orientation (or texture) since surface free energy per unit area of the material varies with respect to crystallographic orientation [53]. Between the Cu-GO coatings with similar texture and grain sizes, the enhancement of the corrosion resistance with increase in GO content can be attributed to the high impermeability of the graphene oxide which can impede the diffusion of the Cu^+ ions across the coating cross-section.

In order to understand their long-term corrosion behaviour, the pure Cu and Cu-GO coatings were exposed to 3.5% NaCl media for 5 days, and subsequently tested in freshly prepared 3.5% NaCl by potentiodynamic polarization. Fig. 5 shows Tafel polarization curves recorded on bare MS, and MS coated with pure Cu, Cu-GO1, Cu-GO2, and Cu-GO3 coatings, after their 5 day long exposure to 3.5% NaCl media. Table 3 provides electrochemical parameters extracted from the Tafel plots shown in Fig. 5. The obtained E_{corr} values on bare MS, Cu/MS, Cu-GO1/MS, Cu-GO2/MS and Cu-GO3/MS were −0.679 V, −0.595 V, −0.545 V, −0.536 V, and −0.458 V respectively. The corresponding i_{corr} values from bare MS, Cu/MS, Cu-GO1/MS, Cu-GO2/MS and Cu-GO3/MS were evaluated to be 316.50, 68.60, 24.07, 13.23, and 10.03 μA cm^{-2} respectively. The corrosion rate values of bare MS, Cu/MS, Cu-GO1/MS, Cu-GO2/MS and Cu-GO3/MS were found to be 144.85, 62.76, 22.08, 12.11, 9.18 mpy respectively. After 5 day long exposure to Cl^- media, all the coatings including bare MS showed increased corrosion rate when compared to their corrosion rate in their as-deposited state. The percentage increase in corrosion rate (%R) due to exposure to Cl^- media was calculated as shown below.

$$\%R = \frac{CR_{exposed} - CR_{as-deposited}}{CR_{as-deposited}} \times 100\ldots, \quad (3)$$

where, $CR_{as\text{-}deposited}$ and $CR_{exposed}$ refer to corrosion rate in the as-deposited state, and after 5 day exposure to Cl^- media respectively.

%R values calculated for bare MS, Cu/MS, Cu-GO1/MS, Cu-GO2/MS and Cu-GO3/MS were about 7%, 9%, 13.5%, 19%, and 51.5% respectively. SEM micrographs in Fig. 6 revealed the surface morphology of the coatings after 5 day exposure to 3.5% NaCl. After 5 day exposure, all the coatings showed an appreciable change in the surface morphology when compared to their as-deposited state. Such change in morphology was clearly due to Cu corrosion from the surface of the coatings.

Table 2
Electrochemical corrosion parameters of as-deposited pure Cu and Cu-GO composite coatings derived Tafel tests.

Sample	β_c (V $decade^{-1}$)	β_a (V $decade^{-1}$)	E_{corr} (V vs Ag-AgCl)	$_{corr}$ (μA cm^{-2})	CR (mil/year)
Bare MS	0.14	0.09	−0.648	295.3	135.15
Cu/MS	0.06	0.32	−0.579	62.89	57.53
Cu-GO1/MS	0.11	0.17	−0.537	21.28	19.46
Cu-GO2/MS	0.11	0.15	−0.505	11.13	10.18
Cu-GO3/MS	0.14	0.11	−0.321	7.24	6.62

Table 3
Electrochemical corrosion parameters of pure Cu and Cu-GO composite coatings after their exposure to 3.5% NaCl for 5 days.

Sample	β_c (V $decade^{-1}$)	β_a (V $decade^{-1}$)	E_{corr} (V vs Ag-AgCl)	i_{corr} (μA cm^{-2})	CR (mil/year)
Bare MS	0.02	0.99	−0.679	316.50	144.85
Cu/MS	0.13	0.20	−0.595	68.60	62.76
Cu-GO1/MS	0.12	0.18	−0.545	24.07	22.08
Cu-GO2/MS	0.14	0.21	−0.536	13.23	12.11
Cu-GO3/MS	0.17	0.19	−0.458	10.03	9.18

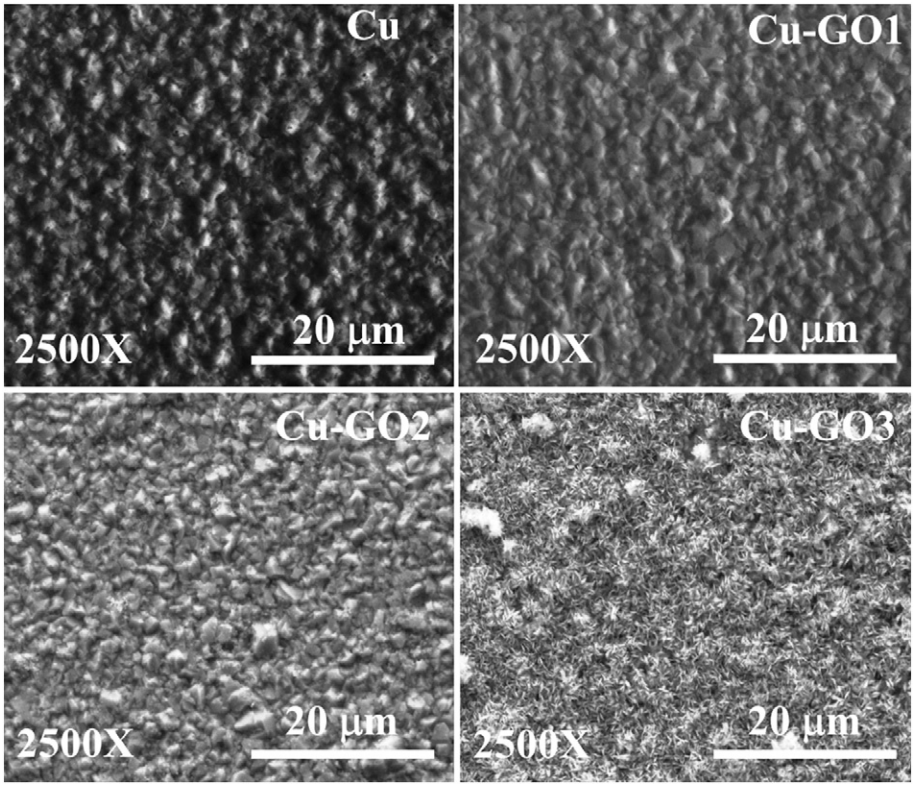

Fig. 6. SEM micrographs showing the surface morphology of pure Cu, and Cu-GO coatings after 5 day exposure to 3.5% NaCl.

The electrochemical behaviour of Cu and Cu-GO coatings during long-term exposure to 3.5% NaCl can be adequately described as follows [27].

$$Cu_2O + H_2O + 4Cl^- \leftrightarrow 2CuCl_2^- + 2OH^- \ldots \quad (3.5)$$

The reduction in corrosion resistance of Cu and Cu-GO upon exposure can be directly attributed to dissolution or breakdown of Cu_2O based passive films caused by aggressive Cl^- ions [27]. According to the reaction (3.5), passive film becomes very unstable against local high concentrations of Cl^- which subsequently leads to its breakdown and gradual removal. Removal of oxide film increases $CuCl_2^-$ concentration close to the film-electrolyte interface. When $CuCl_2^-$ concentrations reach certain threshold value, the backward reaction (hydrolysis) begins to resist the dissolution of oxide film allowing the precipitation of Cu_2O from $CuCl_2^-$ [54]. The net dissolution of passive film is therefore governed by rates at which forward and backward reactions occur at film-electrolyte interface. Though exposed Cu-GO coatings yielded comparatively low corrosion rates, percentage increase in corrosion rate of these coatings was considerably large relative to pure Cu coatings, and increased significantly with GO1, GO2 and GO3. This can be attributed to galvanic coupling between Cu and GO phases. However, it should be noted that the corrosion rates exhibited by Cu-GO coatings after 5 day exposure are substantially small compared to exposed pure Cu coatings. This ascertains that addition of GO in Cu matrix can not only enhance corrosion resistance in the as-deposited state, but also be used to achieve long-term electrochemical stability in aggressive environment such as Cl^-.

A plausible mechanism for enhanced corrosion resistance of Cu-GO coatings is suggested based on the results obtained in this study and a careful review of literature pertinent to Cu corrosion in aerated chloride media [27–29,45–50,52–55]. This mechanism essentially relates to texture induced passivity at the local sites of passivity breakdown, and hence is only valid within the defect sites (such as pits or cracks in the passive film) where Cu corrosion is most likely to occur. A schematic representation given in Fig. 7a illustrates electrochemical corrosion behaviour of pure Cu and Cu-GO coatings in Cl^- media at various intervals of exposure time, namely stages I, II, and III.

Stage I: This corresponds to t = 0, i.e. when the as-deposited coating is brought into contact with Cl^- media. At this stage, it can be fairly assumed that no reactions occur between coating and electrolyte. Cu and Cu-GO coatings are characterised by pre-existing passive film (composed mainly of Cu_2O) with some defects where the passive film becomes vulnerable due to local high Cl^- concentrations. These defects become preferential sites for anodic dissolution of Cu in the following stages.

Stage II: Anodic dissolution of Cu begins preferentially at these defect sites producing cuprous ions (Cu^+) within this defect according to the reaction step **A** (reaction (3.1)). Cu^+ ions subsequently react with Cl^- again to form stable cuprous complexes, $CuCl_2^-$ as shown in the reaction step **B** (reaction (3.3)). The reaction step **C** describes oxygen reduction, which is the main cathodic reaction. At stage II, unlike pure Cu coatings, Cu-GO coatings are shown to exhibit enhanced anodic dissolution (**A**) primarily due to ⟨220⟩ texture. As {220} family of planes possesses greater surface energy per unit area compared to {111} family of planes, Cu-GO coatings are expected to release Cu^+ ions at higher rates [53]. For net accumulation of $CuCl_2^-$ ions to occur within the defect, rate of $CuCl_2^-$ formation should be substantially greater than the rate at which $CuCl_2^-$ diffuses away from the coating-electrolyte interface into the bulk media. Based on this, the concentration of $CuCl_2^-$ ions will rapidly rise within the defect sites in Cu-GO coatings.

Stage III: Once the defect the concentration of $CuCl_2^-$ complexes inside a defect exceeds a threshold value, precipitation of Cu_2O film takes place within the defect as described by the reaction step, **D**

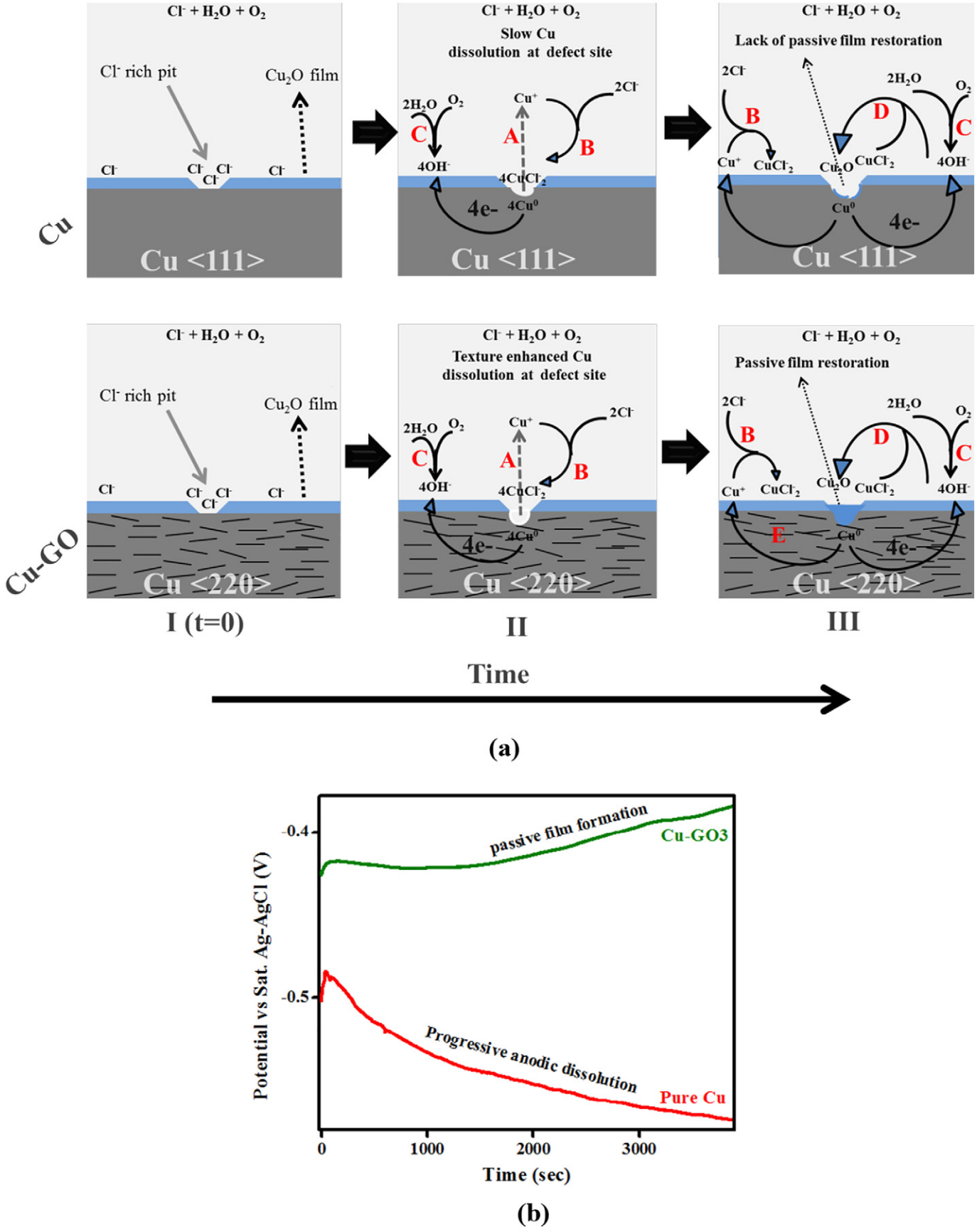

Fig. 7. (a) Schematic illustration of proposed mechanism for enhanced corrosion resistance of Cu-GO composite coatings in Cl^- media, (b) variation in open circuit potential (OCP) of pure Cu and Cu-GO3 coating with exposure time.

(reaction (3.5)) [54]. This restores the passivity at defect sites on Cu-GO coatings. Thus, enhanced anodic dissolution of Cu at defect sites is being proposed as possible mechanism for restoring passivity at the site of film breakdown. **E** refers to the case when the coating is completely covered by passive film. At this point, Cu corrosion is controlled by diffusion of Cu^{+} ions across cross section of the coating and passive film.

Passive film formation via precipitation (reaction step **D**) was confirmed by variation in the open circuit potential (OCP) with immersion time. Fig. 7b shows OCP vs time plots recorded on Cu and Cu-GO3 coatings that were exposed to 3.5% NaCl. Unlike pure Cu whose OCP decreased with time, OCP of Cu-GO3 coating increased with time. Increase in OCP with time indicated passive film formation [55]. Based on this result, it can be concluded that, compared to pure Cu coatings, Cu-GO coatings are generally more stable in 3.5% NaCl owing to stable passive films that can heal up rapidly in the event of localised film damage.

It must be noted that the mechanism discussed above is particularly valid for short exposure times during which the overall passive layer remains intact except in some local defect sites. During long exposure (e.g. several days, week etc.), the passive layer gradually wears away exposing the fresh coating to the media. At this stage, the corrosion of Cu is directly controlled by GO in the coating, which can impede the diffusion of Cu^{+} ions and O_2 across the coating cross section and coating-electrolyte interface owing to high impermeability of GO to ions and tiny molecules [1]. In summary, the electrochemical corrosion results discussed so far clearly demonstrated that addition of GO into Cu matrix can enhance corrosion resistance of Cu metal exposed to aerated Cl^{-} media.

4. Conclusion

An optimized aqueous plating bath consisting of hydrated copper (II) sulphate, SLS (an anionic surfactant), and chemically synthesised GO was employed to electrodeposit highly uniform and compact Cu-graphene oxide composite coatings on MS substrate. Change in the amount of dispersed GO in the bath resulted in Cu-graphene coatings with different GO content. Electrochemical corrosion studies revealed that, when compared to bare steel, the coated steels were less susceptible to corrosive attack in Cl^{-} media. Addition of GO into Cu matrix promoted ⟨220⟩ texture in the composite coatings which remarkably increased their electrochemical resistance when compared to the pure Cu coatings. Additionally, extent of reduction in Cu corrosion rate increased significantly with GO content of the coatings confirming anti-corrosive effect of GO. Texture induced restoration of passivity at local sites of passive film breakdown is suggested as possible mechanism for enhanced corrosion resistance of as-deposited Cu-GO composite coatings. Upon long exposure to Cl^{-} ions, the composite coatings exhibited greater electrochemical stability demonstrating their potential for long-term engineering applications. Based on the electrochemical corrosion studies performed on Cu and Cu-GO coatings, it can be concluded that Cu matrix-GO composite coating can be a promising anti-corrosive coating for long-term corrosion protection of steel in chloride environment such as sea water.

Acknowledgements

Authors acknowledge the research grant received form JATP, IISc (JATP0154).

References

[1] V. Berry, Impermeability of graphene and its applications, Carbon 62 (2013) 1–10.
[2] G. Eda, M. Chhowalla, Chemically derived graphene oxide towards large-area thin-film electronics and optoelectronics, Adv. Mater. 22 (2010) 2392–2415.
[3] A. Ambrosi, C.K. Chua, A. Bonanni, M. Pumera, Electrochemistry of graphene and related materials, ACS Chem. Rev. 114 (2014) 7150–7188.
[4] J. Chen, B. Yao, C. Li, G. Shi, An improved Hummers method for eco-friendly synthesis of graphene oxide, Carbon 64 (2013) 225–229.
[5] A.S. Sai Pavan, S.R. Ramanan, A study on corrosion resistant graphene films on low alloy steel, Appl. Nanosci. (2016)http://dx.doi.org/10.1007/s13204-016-0530-2.
[6] M. Zhu, Z. Du, Z. Yin, W. Zhou, Z. Liu, S.H. Tsang, E.H.T. Teo, Low-temperature in situ growth of graphene on metallic substrates and its application in anticorrosion, ACS Appl. Mater. Interfaces 8 (2016) 502–510.
[7] F. Zhou, Z. Li, G.J. Shenoy, L. Li, H. Liu, Enhanced room-temperature corrosion of copper in the presence of graphene, ACS Nano 7 (2013) 6939–6947.
[8] S. Chen, L. Brown, M. Levendorf, W. Cai, S.Y. Ju, J. Edgeworth, X. Li, C.W. Magnuson, A. Velamakanni, R.D. Piner, J. Kang, J. Park, R.S. Ruoff, Oxidation resistance of graphene-coated Cu and Cu/Ni alloy, ACS Nano 5 (2011) 1321–1327.
[9] K.C. Chang, M.H. Hsu, H.-I. Lu, M.C. Lai, P.J. Liu, C.H. Hsu, W.-F. Ji, T.L. Chuang, Y. Wei, J.M. Yeh, W.-R. Liu, Room-temperature cured hydrophobic epoxy/graphene composites as corrosion inhibitor for cold-rolled steel, Carbon 66 (2014) 144–153.
[10] W. Sun, L. Wang, T. Wu, Y. Pan, G. Liu, Synthesis of low-electrical-conductivity graphene/pernigraniline composites and their application in corrosion protection, Carbon 79 (2014) 605–614.
[11] B.P. Singh, S. Nayak, K.K. Nanda, B.K. Jena, S. Bhattacharjee, L. Besra, The production of a corrosion resistant graphene reinforced composite coating on copper by electrophoretic deposition, Carbon 61 (2013) 47–56.
[12] C.-H. Chang, T.-C. Huang, C.-W. Peng, T.-C. Yeh, H.-I. Lu, W.-I. Hung, C.-J. Weng, T.-I. Yang, J.-M. Yeh, Novel anticorrosion coatings prepared from polyaniline/graphene composites, Carbon 50 (2012) 5044–5051.
[13] B. Ramezanzadeh, E. Ghasemi, M. Mahdavian, E. Changizi, M.H.M. Moghadam, Covalently-grafted graphene oxide nanosheets to improve barrier and corrosion protection properties of polyurethane coatings, Carbon 93 (2015) 555–573.
[14] B. Ramezanzadeh, S. Niroumandrad, A. Ahmadi, M. Mahdavian, M.H.M. Moghadam, Enhancement of barrier and corrosion protection performance of an epoxy coating through wet transfer of amino functionalized graphene oxide, Corros. Sci. 103 (2016) 283–304.
[15] K. Qi, Y. Sun, H. Duan, X. Guo, A corrosion-protective coating based on a solution-processable polymer-grafted graphene oxide nanocomposite, Corros. Sci. 98 (2015) 500–506.
[16] Z. Yu, H. Di, Y. Ma, L. Lv, Y. Pan, C. Zhang, Y. He, Fabrication of graphene oxide–alumina hybrids to reinforce the anti-corrosion performance of composite epoxy coatings, Appl. Surf. Sci. 351 (2015) 986–996.
[17] B.P. Singh, B.K. Jena, S. Bhattacharjee, L. Besra, Development of oxidation and corrosion resistance hydrophobic graphene oxide-polymer composite coating on copper, Surf. Coat. Technol. 232 (2013) 475–481.
[18] M.Y. Rekha, M.K. Punith Kumar, C. Srivastava, Electrochemical behaviour of chromium–graphene composite coating, RSC Adv. 6 (2016) 62083–62090.
[19] R. Berlia, M.K. Punith Kumar, C. Srivastava, Electrochemical behavior of Sn–graphene composite coating, RSC Adv. 5 (2015) 71413–71418.
[20] D. Prasai, J.C. Tuberquia, R.R. Harl, G.K. Jennings, K.I. Bolotin, Graphene: corrosion-inhibiting coating, ACS Nano 6 (2012) 1102–1108.
[21] M. Schriver, W. Regan, W.J. Gannett, A.M. Zaniewski, M.F. Crommie, A. Zettl, Graphene as a long-term metal oxidation barrier: worse than nothing, ACS Nano 7 (2013) 5763–5768.
[22] S. Pei, H.M. Cheng, The reduction of graphene oxide, Carbon 50 (2012) 3210–3228.
[23] M.K. Punith Kumar, C. Srivastava, Electrochemical behavior of Zn–graphene composite coatings, Mater. Charact. 85 (2013) 82–91.
[24] M. Dutta, A.K. Halder, S.B. Singh, Morphology and properties of hot dip Zn–Mg and Zn–Mg–Al alloy coatings on steel sheet, Surf. Coat. Technol. 205 (2010) 2578–2584.
[25] S. Schuerz, M. Fleischanderl, G.H. Luckeneder, K. Preis, T. Haunschmied, G. Mori, A.C. Kneissl, Corrosion behaviour of Zn-Al-Mg coated steel sheet in sodium chloride-containing environement, Corros. Sci. 51 (2009) 2355–2363.
[26] T. Prosek, A. Nazarov, U. Bexell, D. Thierry, J. Serak, Corrosion mechanism of model zinc–magnesium alloys in atmospheric conditions, Corros. Sci. 50 (2008) 2216–2231.
[27] G. Kear, B.D. Barker, F.C. Walsh, Electrochemical corrosion of unalloyed copper in chloride media—a critical review, Corros. Sci. 46 (2004) 109–135.
[28] F. Mansfeld, G. Liu, H. Xiao, C.H. Tsai, B.J. Little, The corrosion behavior of copper alloys, stainless steels and titanium in seawater, Corros. Sci. 36 (1994) 2063–2095.
[29] J. Mathiyarasu, N. Palaniswamy, V.S. Muralidharan, Electrochemical behaviour of copper-nickel alloy in chloride solution, J. Chem. Sci. 111 (1999) 377–386.
[30] J. Elguindy, S. Moffitt, H. Hasman, C. Andrade, S. Raghavan, C. Rensing, Metallic copper corrosion rates, moisture content, and growth medium influence survival of copper ion-resistant bacteria, Appl. Microbiol. Biotechnol. 89 (2011) 1963–1970.
[31] Z.A. Hamid, A.A. Aal, New environmentally friendly noncyanide alkaline electrolyte for copper electroplating, Surf. Coat. Technol. 203 (2009) 1360–1365.
[32] S. Miura, H. Honma, Advanced copper electroplating for application of electronics, Surf. Coat. Technol. 169–170 (2003) 91–95.
[33] L.L. Barbosa, M.R.H. De Almeida, R.M. Carlos, M. Yonashiro, G.M. Oliveira, I.A. Carlos, Study and development of an alkaline bath for copper deposition containing sorbitol as complexing agent and morphological characterization of the copper film, Surf. Coat. Technol. 192 (2005) 145–153.
[34] D.R. Dreyer, S. Park, C.W. Bielawski, R.S. Ruoff, The chemistry of graphene oxide, Chem. Soc. Rev. 39 (2010) 228–240.
[35] J. Zhang, H. Yang, G. Shen, P. Cheng, J. Zhang, S. Guo, Reduction of graphene oxide via L-ascorbic acid, Chem. Commun. 46 (2010) 1112–1114.
[36] D. Grujicic, B. Pesic, Electrodeposition of copper: the nucleation mechanisms, Electrochim. Acta 47 (2002) 2901–2912.
[37] N.M. Martyak, Characterization of thin electroless nickel coatings, Chem. Mater. 6 (1994) 1667–1674.

[38] M.S. Sabri, A.A. Sarabi, S.M.N. Kondelo, The effect of sodium dodecyl sulfate surfactant on the electrodeposition of Ni-alumina composite coatings, Mater. Chem. Phys. 136 (2012) 566–569.
[39] J. Sudagar, J.S. Lian, Q. Jiang, Z.H. Jiang, G.Y. Li, R. Elansezhian, The performance of surfactant on the surface characteristics of electroless nickel coating on magnesium alloy, Prog. Org. Coat. 74 (2012) 788–793.
[40] L. Alexander, H.P. Klug, Determination of crystallite size with X-ray spectrometer, J. Appl. Phys. 21 (1950) 137–142.
[41] C.M. Praveen Kumar, T.V. Venkatesha, R. Shabadi, Preparation and corrosion behavior of Ni and Ni graphene composite coatings, Mater. Res. Bull. 48 (2013) 1477–1483.
[42] N.T. Kirkland, T. Schiller, N. Medhekar, N. Birbilis, Exploring graphene as a corrosion protection barrier, Corros. Sci. 56 (2012) 1–4.
[43] M. Bagherzadeh, Z.S. Ghahfarokhi, E.G. Yazdi, Electrochemical and surface evaluation of the anti-corrosion properties of reduced graphene oxide, RSC Adv. 6 (2016) 22007–22015.
[44] Y. Raghupathy, K.A. Natarajan, C. Srivastava, Anti-corrosive and anti-bacterial properties of nanocrystalline Ni-Ag coatings, Mater. Sci. Eng. B 206 (2016) 1–8.
[45] G. Bianchi, P. Longhi, Copper in sea-water, potential-pH diagrams, Corros. Sci. 13 (1973) 853–864.
[46] F. Arjmand, A. Adriaens, Influence of pH and chloride concentration on the corrosion behavior of unalloyed copper in NaCl solution: a comparative study between the micro and macro scales, Materials 5 (2012) 2439–2464.
[47] J.K. Yu, E.H. Han, L. Lu, X.J. Wei, M. Leung, Corrosion behavior of nanocrystalline and conventional polycrystalline copper, Mater. Sci. 40 (2005) 1019–1022.
[48] W. Luo, Y. Xu, Q. Wang, P. Shi, M. Yan, Effect of grain size on corrosion of nanocrystalline copper in NaOH solution, Corros. Sci. 52 (2010) 3509–3513.
[49] W. Luo, C. Qian, X.J. Wu, M. Yan, Electrochemical corrosion behavior of nanocrystalline copper bulk, Mater. Sci. Eng. A 452 (2007) 524–528.
[50] E.M. Sherif, Inhibition of copper corrosion reactions in neutral and acidic chloride solutions by 5-ethyl-1,3,4-thiadiazol-2-amine as a corrosion inhibitor, Int. J. Electrochem. Sci. 7 (2012) 2832–2845.
[51] K.M. Ismail, A.M. Fathi, W.A. Badawy, Electrochemical behavior of copper–nickel alloys in acidic chloride solutions, Corros. Sci. 48 (2006) 1912–1925.
[52] H. Otmacic, E. Stupnisek-Lisac, Copper corrosion inhibitors in near neutral media, Electrochim. Acta 48 (2003) 985–991.
[53] E. Martinez-Lombardia, Y. Gonzalez-Garcia, L. Lapeire, I.D. Graeve, K. Verbeken, L. Kestens, J.M.C. Mol, H. Terryn, Electrochim. Acta 116 (2014) 89–96.
[54] M. M-Hukovic, R. Babic, I. Škugor, Z. Grubac, Copper–nickel alloys modified with thin surface films: corrosion behaviour in the presence of chloride ions, Corros. Sci. 53 (2011) 347–352.
[55] M.M. Antonijevic, S.C. Alagic, M.B. Petrovic, M.B. Radovanovic, A.T. Stamenkovic, The influence of pH on electrochemical behavior of copper in presence of chloride ions, Int. J. Electrochem. Sci. 4 (2009) 516–524.